Journal of Alloys and Compounds 509 (2011) 3582–3586

Contents lists available at ScienceDirect

Journal of Alloys and Compounds

journal homepage: www.elsevier.com/locate/jallcom

Structural investigations of oxidative behavior on nanocrystalline nickel

Soumen Kar[a], Vidyadhar Singh[b,*]

[a] Cryogenic Engineering Centre, Indian Institute of Technology, Kharagpur 721302, West Bengal, India
[b] Department of Physics and Meteorology, Indian Institute of Technology, Kharagpur 721302, West Bengal, India

ARTICLE INFO

Article history:
Received 2 August 2010
Received in revised form 9 December 2010
Accepted 12 December 2010
Available online 21 December 2010

Keywords:
Oxidation
Mechanical alloy
Thermal
Magnetic properties

ABSTRACT

We have reported a comprehensive study of the structural, magnetic and electrical properties of Ni (core)/NiO (shell) particles, synthesized by control oxidation of ball milled nanocrystalline (nc-) Ni particles in air. A reaction of $Ni + (1/2)O_2 \rightarrow NiO$ is suspected to occur in the oxidation reaction at the temperature range of 300–800 °C. The phases of the Ni/NiO particles are composed of fcc-Ni and fcc-NiO. The phase compositions of the Ni/NiO particles change with annealing temperature. The Ni/NiO particles have a core–shell monomorphic flower-like microstructure with an average diameter of 20–80 nm. The size reduction and oxidation of the nc-Ni particles leads to a change in microstructure and thermal stability compared to bulk Ni. Thermogravimetric and differential scanning calorimetery analysis are applied to determine the thermal behavior of composites. The initial oxidation of nc-Ni particles is observed to occur around 325 °C (near Curie temperature). Anomalous magnetic and electric behavior is observed at room temperature for the nc-Ni and Ni/NiO particles.

1. Introduction

Studies on nanometer-sized metal/metal-oxide particles (nanoparticles) have progressed rapidly over the past decade [1–5]. Ni and/or NiO are receiving increased attention for not only their interesting chemical characteristic, such as catalysts, fuel cell electrodes, gas sensors and supercapacitors/battery hybrids but also for their magnetic properties since NiO is antiferromagnetic and Ni is ferromagnetic [1–10]. In addition, metal–ceramic materials are also interesting since they typically exhibit enhanced mechanical properties [6]. The frequently encountered obstacle during the preparation of nanoscale metal particles is the spontaneous production of oxides due to very high surface to volume ratio of the particles. As a result, metal particles are being encapsulated within a spontaneous surface oxide (SSO) layer, which is known as a 'core–shell' structure [7,8]. For example, in many solar absorbing coatings, the presence of a dielectric/insulating shell at least part of the metallic core severely delays the oxidation and appears to be the main reason for their high stability [9]. In addition to this, when ferromagnetic (FM) particles are embedded in a metal, semi-conducting or insulator matrix, the matrix is expected to introduce an extra degree of freedom that can be used to tune the properties of the embedded particles or the composite as a whole [10]. It is an irrefutable fact that a passivating oxide layer on FM particle plays a crucial role in magnetic properties. However, one major disadvantage is that the oxide coating close to the transition metallic core (e.g., Fe, Co, Ni) weakens in the exchange interactions of the surface atoms with the surrounding ones thereby modifying the magnetism and other related properties to an appreciable extent [8]. Apart from the oxide layer, the magnetization of nanocrystalline ferromagnets is also reported to be highly sensitive to oxygen contamination. A rough estimate shows that every oxygen atom destroys the contribution of one Ni atom to ferromagnetism and leads to a strong decrease of magnetization. The SSO layer and absorbed oxygen in magnetic nanoscale particles thus itself justifies an in-depth study. Therefore, there have also been studies on transition metal–transition metal oxide systems (Ni–NiO, Fe–FeO and Co–CoO) where the magnetic, optical and electrical transport characteristics can be tailored by changing the relative dimensions of the core and shell in the particles [11–17]. They are in the size range of 20–200 nm. Thus, it is important to understand and compare the intrinsic physical properties of Ni/NiO with those of nanocrystalline Ni. The oxidation of Ni particles ($Ni + (1/2)O_2 \rightarrow NiO$) is a reaction with highly important and technological significance [18,19].

More profoundly at the nanometer scale, metal particles are typically covered by passivated films to protect them from further oxidation, the composition and thickness of these layers play significant roles in the oxidation process. The characterization and elemental analysis of these oxide layers, however, are apparently neglected in most of the studies, which might be one primary reason for the different results reported. In order to advance understanding of oxidation behavior at the nanometer scale, this study

* Corresponding author. Tel.: +91 03222281637.
E-mail addresses: soumen@hijli.iitkgp.ernet.in (S. Kar), vsingh@phy.iitkgp.ernet.in (V. Singh).

0925-8388/$ – see front matter © 2010 Elsevier B.V. All rights reserved.
doi:10.1016/j.jallcom.2010.12.077

will focus on an experimental investigation of complete oxidation of nickel particles based on the isoconversion method. Mechanical milling is a well-known technique, largely used in a wide range of processes [20]. In mechanical treatments carried out by ball-milling, powder particles are subjected to a severe plastic deformation due to the repetitive compressive loads arising from the impacts between the balls and the powder. For example, the extension of the solid solubility limits, the production of intermetallic compounds with crystallite sizes at the nanometer scale, or the synthesis of novel crystalline and amorphous materials has been reported. An alternative to nanostructured thin-film approach is the utilization of magnetic particles embedded in an antiferromagnetic (AFM) matrix [6]. Such core–shell composites have the added benefits of: (i) lower resistivity (controlled by the interparticle distance), and hence, reduced eddy-current losses, and (ii) the ability to tailor the magnetic properties of the composite system by control of the physical properties (such as the size, shape, orientation, and volume fraction) of the particles.

This paper presents the results of an investigation into the synthesis of nanoparticulate Ni by mechanical processing and simultaneous oxidation behavior at 300–800 °C. The role of the NiO shell thickness on the thermal stability of nanocrystalline Ni is also discussed. We contribute it to the microstructural effect induced by the control oxidation. Further, the room temperature magnetic and electrical resistivity behavior on these particles has been investigated.

2. Experimental details

Ball milling technique has been adopted to synthesize nc-Ni particles with sizes down to average diameter of 30 nm from the as-purchased (AP) Ni powders. The AP-nickel particles are about spherical with a wide size distribution between 5 and 10 μm (99.9%, Alfa Aesar). The ball milling technique helps in forming nc-Ni by reducing the particle size. The AP-Ni particles have been mechanically milled in a high-energy planetary ball milling (RETSCH PM-200) by introducing a centrifugal force. Milling has been performed in toluene using tungsten carbide (WC) milling medium. The diameter of each ball is 10 mm. The ball to powder ratio is maintained at 10:1 and the milling is done at 300 rpm for 60 h. This is the first attempt in which Ni powders are made in liquid medium (toluene) instead of Argon, where the toluene acts as a coolant and reduces the surface (contamination) oxidation. Subsequently, the milled powders are subjected to isothermal annealing in air at various temperatures between 300 and 800 °C for 1 h to form a spontaneous surface oxide layer of NiO, which encapsulates the Ni particles as they have been prepared under ambient atmosphere. The relative change in mass ($\Delta M/M$) at room temperature is measured after annealing of the ball milled Ni sample at different temperatures using a highly sensitive (±1 μg) digital balance (CP 225D-SARTORIOUS). The structure and phase of the as-milled and annealed samples have been studied by high resolution X-ray diffraction (XRD) using Pan-analytical X'pert Pro-XRD system (PW 3040), with filtered Cu $K\alpha_1$ radiation of wavelength $\lambda = 0.15406$ nm. The crystallite size and microstrain of as-milled and annealed powders are estimated by applying Williamson–Hall method [21,22],

$$\beta \cos\theta = 2\varepsilon \sin\theta + \frac{K\lambda}{D} \quad (1)$$

where β is the full-width at half-maximum of the diffraction peak, θ is the Bragg angle, λ is the wavelength of the X-ray, D is the crystallite size and ε is the internal microstrain produced during milling. Thermogravimetric (TG) and differential scanning calorimeter (DSC) measurements have been performed by heating as-milled and air-annealed Ni samples over a range of 30–800 °C at a heating rate of 10 K/min under air using TG/DSC–Perkin Elmer instruments. The particle size, morphology and chemical compositions are evaluated by a transmission electron microscope (TEM) with an acceleration voltage of 200 kV (JEOL, JEM-2100) and energy-dispersive X-ray spectrometer (EDS). The magnetization data as a function of applied fields up to 8 kOe is recorded using vibrating sample magnetometery (VSM). The room temperature electrical resistivity measurements are carried out using standard four probe DC resistivity (for smaller resistance value) method and two probe DC resistivity (for higher resistance value) method.

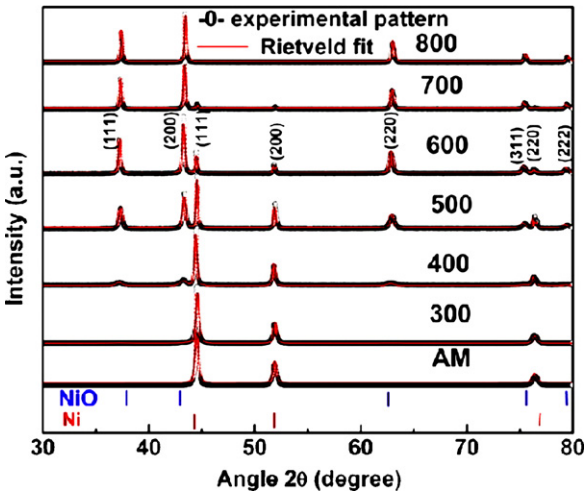

Fig. 1. X-ray diffraction patterns of the as-milled and annealed of nc-Ni powder at 300, 400, 500, 600, 700 and 800 °C in air for 1 h, along with the Rietveld fits. The profiles calculated from the fitting procedure are displayed as a continuous line while the symbols (○) are the experimental points.

3. Results and discussion

Fig. 1 shows the XRD spectra of as-milled nc-Ni sample and of the air-annealed Ni/NiO samples. The patterns of as-milled and 300 °C air-annealed samples are characteristic of the pure face centered cubic (fcc)-Ni phase. In the XRD spectra of the 400 °C sample shows growth in fcc-NiO phase along with the decrease in the Ni peak intensity. In XRD patterns no other impurities are found but it is also confirmed from EDS analysis. In EDS analysis some carbon/tungsten is found which is derived from the mechanical abrasion of the WC vial and balls. Characterization of microstructure of these nanocomposites is carried out employing Rietveld's analysis. In the present study, the most suitable pseudo-Voigt analytical function [23] is adopted for fitting of the experimental profiles. The XRD patterns have been analyzed using Rietveld analysis (Fig. 1), providing the volume averaged crystallite size, microstrain and weight fraction of the detected phases. The principal results are summarized in Table 1. For all the Rietveld analyses, the R-weighted pattern (R_{wp}), this is a useful indicator of the goodness of the fit. It is close to 10%, indicating a rather high reliability of the results. The as-milled Ni is without any formation of NiO, it means that only fcc-Ni with a crystallite size of 26 nm is obtained, even microstrain is increased from 0.023% to 0.103% in compare to AP-Ni. This much microstrain is released when annealing of nc-Ni is done at different temperatures. When the Ni is completely transformed to NiO then strain

Table 1
Results of microstructure in as-milled nc-Ni and annealed Ni/NiO particles revealed from Rietveld's and Williamson–Hall X-ray powder diffraction line profile.

Sample	As-milled	300 °C		400 °C		500 °C		600 °C		700 °C		800 °C
	Ni	Ni	NiO	Ni	NiO	Ni	NiO	Ni	NiO	Ni	NiO	NiO
Crystallite size (nm)	31	33	7	47	15	74	31	97	46	113	61	65
Micro strain%	0.103	0.09	0.9	0.07	0.22	0.04	0.1	0.03	0.07	0.02	0.05	0.05
Weight%	100	97	3	71	29	36	64	13	87	4	96	100
$V/10^6$ pm^3	43.81	43.78	73.43	43.75	72.82	43.73	72.82	43.76	72.89	3.78	72.91	72.92
R_p (profifile)/%	2.46	2.61		2.27		3.40		2.70		2.49		2.38
R_{wp} (wt. proffile)/%	1.93	1.85		1.87		2.42		1.87		1.83		1.80

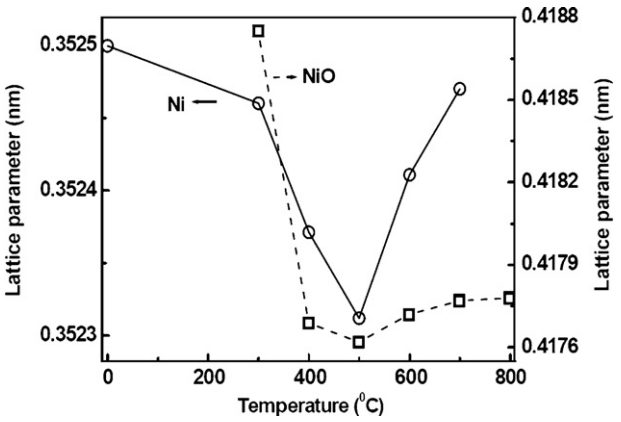

Fig. 2. Dependence of the lattice parameters of NiO and Ni on annealing temperature. The lines are guides to the eye.

is also decreased with a crystallite size of 65 nm for NiO. It means that the increase in annealing temperature, the weight fraction of core part (Ni) is diminished, and the thicker shell part (NiO) hence weight fraction of NiO is increased. The change in lattice parameter also shows an interesting result which is shown in Fig. 2. It is observed from Fig. 2 that the lattice parameter starts to decrease as the annealing temperature increases for both Ni and NiO but there is an optimum value of the lattice parameter at 500 °C. After that the lattice parameter starts to increase once again with the increase in annealing temperature for both Ni and NiO.

It is known as the Curie temperature (T_C) of Ni is 354.6 °C [24,25]. To find out precisely at what temperature it happens, the thermal evolution of the phase is studied for both DSC and TG techniques in the presence of air. Fig. 3(a) and (b) shows DSC and TG profiles of the as-milled nc-Ni and annealed Ni/NiO samples. A sharp exothermic peak at 334 °C has been observed for as-milled sample. However, a broad exothermic peak at 334 °C has been observed in case of the 400 and 500 °C annealed samples. Further at higher temperature annealed (800 °C) samples, that peak has been disappeared. The broad exothermic peak for 400 and 500 °C annealed Ni/NiO samples are probably due to the crystallization of any amorphous species present in the surface layers. The sharp exothermic peak at 334 °C for as-milled sample shows the release of strain energy and the transformation to NiO phase. The mass loss% and T_C variations with annealing temperature is shown in the inset of Fig. 3(b) and this clearly shows an increase in T_C with the annealing temperature. In the case of mass loss%, it is observed that initially mass loss% is increasing but as the annealing temperature is increasing mass loss% is decreasing because of dissolved oxygen in it. The TG curve shows a steep rise with a 20% weight increase in the as-milled at 334 °C, confirming further production of oxide layer above T_C. The increase in mass loss% is further increased to 23% for 400 °C annealed Ni/NiO sample because the dissolved surface oxygen atoms are removed at 470 °C thus it increase the intake of more oxygen atoms to create more thicker oxide shell over Ni core. For high temperature annealed Ni/NiO samples, increase in mass loss% is less because of the existence of thicker oxide shell over Ni core and the peak variation also occur due to the passivated oxygen layer in its surface. The coexistence of Ni and NiO in these oxidized samples has been observed in XRD and TEM and afterward it is confirmed by the magnetization measurements. For as-milled nc-Ni sample, the onset of ferromagnetism is observed below a T_C of 334 °C, which is almost compared as bulk Ni. There is an increase in T_C has been observed for the annealed Ni/NiO samples. It is believed that strains due to the Ni and NiO lattice constant arise at the interface. For an ultra thin oxide layer (NiO shell) over the Ni (Core), the strain is more significant which is perceived for 400 °C annealed

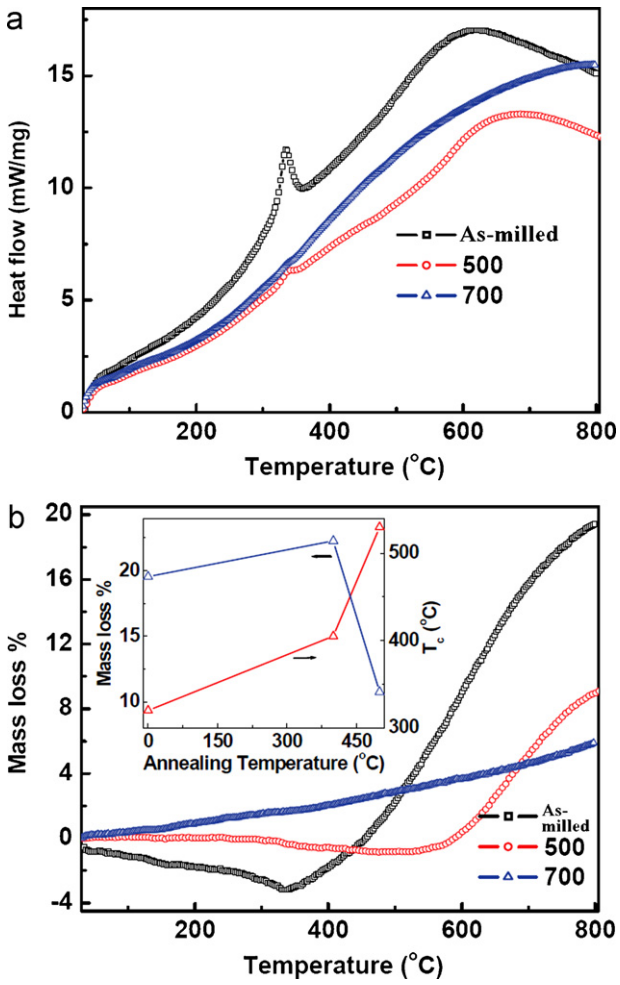

Fig. 3. (a) DSC and (b) TG profile of as-milled (nc-Ni), 500 and 700 °C (Ni/NiO) annealed (Ni/NiO) samples. The variation in mass loss% and T_C with annealing temperature is shown in the inset (b).

Ni/NiO sample. In many cases, interface strain in thin NiO layers leads to a suppression of T_C [26], however, the increase of T_C found in the annealed Ni/NiO samples suggests instead that the strain is less directional, and acts more like hydrostatic pressure, known to increase T_C in bulk Ni [27].

Fig. 4(a) shows a bright field TEM image of the as-milled Ni sample with selected area electron diffraction (SAED) pattern (inset). SAED pattern of as-milled nc-Ni [inset of Fig. 4(a)] consists of four rings with spots from (1 1 1), (2 0 0), (2 2 0) and (3 1 1) reflections of fcc-Ni in accordance to the XRD pattern. The nc-Ni particles have a spherical shape with an average diameter of 20 nm. Fig. 3(b–d) presents the TEM images of 400, 500 and 700 °C annealed Ni/NiO samples, which clearly shows the crystalline nature of core (Ni) and a shell (NiO). The particles show a monomorphic and uniform core–shell structure with flower-like shape. The particle sizes of Ni/NiO particles are found in the range from 50 to 200 nm. In Fig. 3(c) the SAED pattern of 400 °C annealed does not show nanocrystalline behavior due to grain growth at higher temperature annealing. This microstructure results are further supported by the magnetic and electrical resistivity data discussed in the following section.

The magnetic behavior of as-milled nc-Ni and annealed Ni/NiO samples has been assessed through magnetization data taken at room temperature. Fig. 5 shows the variation of magnetization (M) as a function of applied field (H) for the as-milled nc-Ni and annealed Ni/NiO samples. M–H curves for the as-milled nc-Ni

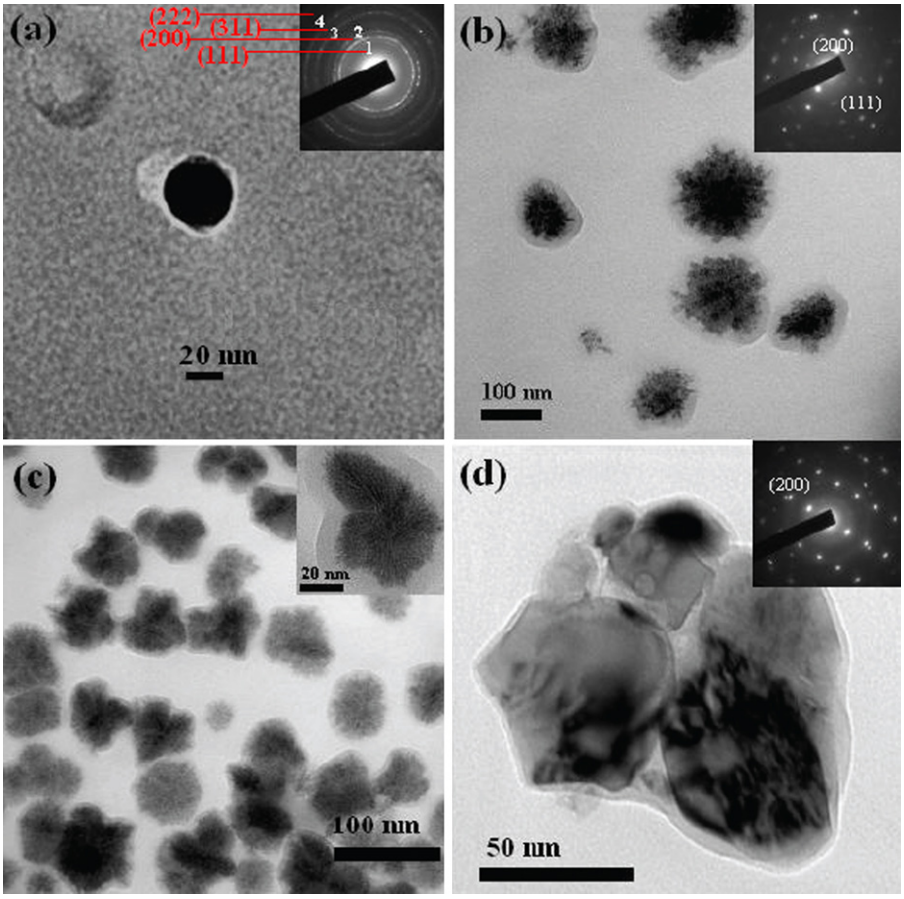

Fig. 4. TEM images of (a) as-milled (nc-Ni), (b) 400 °C, (c) 500 °C and (d) 700 °C annealed (Ni/NiO) powders samples with SAED pattern in the insets.

samples yield the saturation magnetization (M_S), remanent magnetization (M_r), and coercivity (H_C) of 46.7 emu/g, 12.6 emu/g, and 115 Oe, respectively. The M_S-value of as-milled nc-Ni is still lower than bulk-Ni value (55.0 emu/g) due to the nanosize effect. The 600 and 700 °C annealed Ni/NiO samples presume low magnetization, which does not saturate up to the field used here, in predominance of the NiO in accordance to the XRD pattern. At low fields, the magnetization increases rapidly followed by a moderate nonlinear value, and then a high-field linear behavior. This behavior of the samples is suggesting the coexistence of a FM phase (Ni) and an AFM/PM (NiO) phase. The *M–H* curves are fitted to the following equation comprising of FM and AFM/PM part suggested by Stearns and Cheng [28]

$$M(H) = \frac{2M_S}{\pi} \tan^{-1}\left[\frac{H \pm H_C}{H_C} \tan\left(\frac{\pi S}{2}\right)\right] + \chi H \quad (2)$$

The first term is the usual function customarily used to fit FM hysteresis curves while the second term accounts for the AFM/PM component with χ as the magnetic susceptibility. The quantities M_S and H_C give respectively the saturation magnetization of the FM component and coercivity of the hysteresis loop. '*S*' is known as 'squareness' of the FM loop and is defined as the ratio of remnant magnetization to saturation magnetization of the FM component i.e., $S = M_r/M_S$. Reasonably good fits to the magnetization curves have been obtained for all samples which are shown in Fig. 5. Table 2

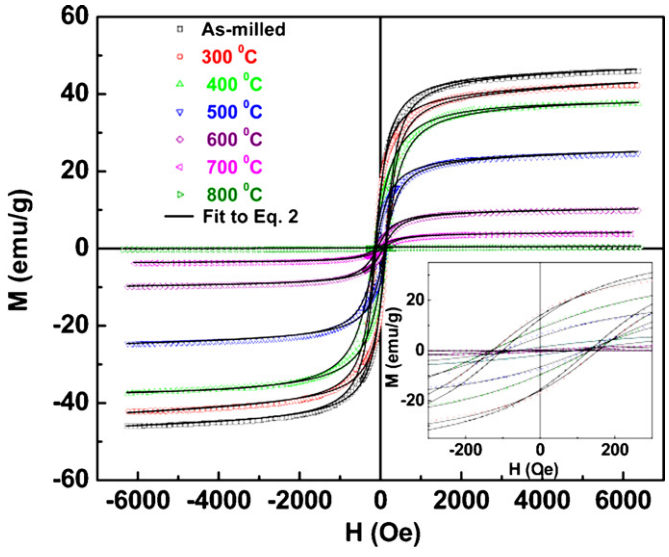

Fig. 5. *M–H* curves measured at room temperature for as-milled (nc-Ni) and annealed (Ni/NiO) samples with fit of Eq. (2). Inset shows the *M–H* curves at low fields.

Table 2
Parameters extracted from fitting Eq. (2) of *M–H* data for as-milled nc-Ni and annealed Ni/NiO samples.

Sample	Phase	M_S (emu/g)	H_C (Oe)	S (M_r/M_S)	χ (emu/g Oe)
As-milled	Ni	46.7	115	0.27	2.4×10^{-4}
300 °C	Ni–NiO	42.8	130	0.34	2.2×10^{-4}
400 °C	Ni–NiO	39.3	170	0.41	1.7×10^{-4}
500 °C	Ni–NiO	24.2	117	0.22	1.3×10^{-4}
600 °C	Ni–NiO	9.7	87	0.13	1.0×10^{-4}
700 °C	Ni–NiO	3.8	47	0.08	4.0×10^{-4}
800 °C	Ni–NiO	0.15	28	0.05	2.0×10^{-4}

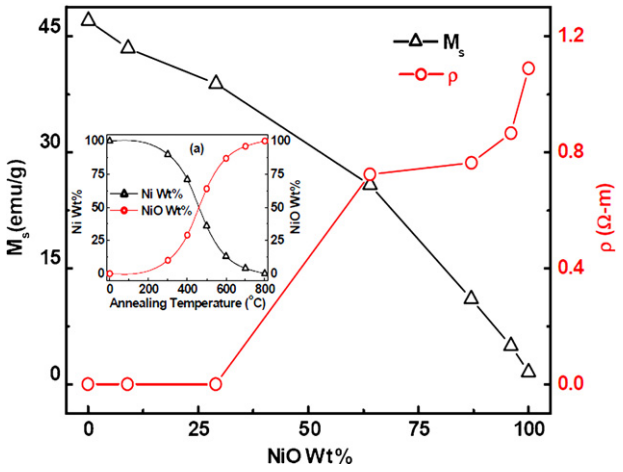

Fig. 6. The saturation magnetization and resistivity dependence of Ni and NiO on annealing temperature with NiO weight%. Inset shows the Ni and NiO weight% with annealing temperature.

compares the magnitude of S, H_C, M_S and χ for as-milled nc-Ni and annealed Ni/NiO samples as obtained from the fits. For example, the FM and PM parts so obtained for 300, 400 and 500 °C annealed Ni/NiO are given in Table 2, with $S = 0.34$, 0.41 and 0.22, respectively. The smaller S-values relative comparison to an ideal value 0.5 in randomly oriented ideal single ferromagnetic domains suggests that FM Ni (core) particles are interacting via an AFM phase of the SSO layer (NiO). The analysis confers that the surface layer is playing an important role in determining the final magnetic properties. The enhancement in H_C value at intermediate temperatures (400 °C) is compared with as-milled nc-Ni, indicates the existence of a Ni–NiO core–shell structure, which is in agreement with the structural data. The decrease in magnetization on annealing in air (Fig. 6b) point out the increased content of NiO in samples (see inset Fig. 6). In addition to the production of core–shell structure an exchange bias effect in the interface of the Ni/NiO layer would be interesting which is reported in some earlier reports [1,5].

Electrical resistivity provides strong evidence for the charge and orbital ordering transition when the sample enters to an insulating state on charge ordering. Often the charge ordering transition is reflected as a change in slope in the resistive plot. In the present investigation, particularly electrical resistivity (ρ) as a function of annealing temperature is shown in Fig. 6 for as-milled nc-Ni and annealed Ni–NiO pellet samples. The as-milled nc-Ni sample shows a typical metallic behavior with higher ρ values (5.43 μΩ cm) compared to bulk Ni (6.85 μΩ cm). When the nc-Ni sample is annealed above 400 °C, the ρ values (28.6 μΩ cm) increase quite significantly, indicating the formation of thicker surface NiO layer that can result in a combination of metallic and insulating behavior. The magnetic and electrical properties are consistent the Ni and NiO weight% with annealing temperature (inset of Fig. 6).

4. Conclusions

In summary, we have studied the microstructural, magnetic and electrical properties of nc-Ni particles after annealing under air with temperatures up to 800 °C. Nanosized Ni particles have been synthesized using ball milling technique. The XRD patterns of Ni/NiO particles have been indexed as fcc crystal structure. The XRD pattern showed an interesting feature that Ni peak intensities are decreased with an increasing of NiO peaks, while annealing temperature is near Curie temperature of nc-Ni. TEM studies of Ni/NiO particles show a monomorphic and uniform core–shell structure with flower-like shapes are formed by control oxidation of nc-Ni in the temperature range of 300–800 °C. The particle size of Ni/NiO particles are found in the range from 50 nm to 200 nm. From the magnetic study, it is observed that the magnetization values are decreasing as the annealing temperature is increasing and it is due to an increase in the fraction of AFM phase of NiO. The absolute resistivity increases as temperature of annealing increases and this is due to an increase in the fraction of insulating phase made of NiO. This study helps one to understand the influence of oxidation on the microstructure and enhanced properties of nc-Ni particles.

Acknowledgements

Authors thank Prof. V. Srinivas (Physics Department, IIT, Kharagpur) and Prof. N.K. Kishore (Electrical Engineering Department, IIT, Kharagpur) for the helpful discussions. This work was supported by Armament Research Board, DRDO and Ministry of Human Resources & Development (MHRD), New Delhi, India. V. Singh gratefully acknowledges the CSIR, Government of India, for a Senior Research Fellowship.

References

[1] L. Del Bianco, F. Boscherini, A.L. Fiorini, M. Tamisari, F. Spizzo, M. Vittori Antisari, E. Piscopiello, Phys. Rev. B 77 (2008) 094408.
[2] V. Srinivasan, J. Weidner, J. Electrochem. Soc. 144 (1997) L210.
[3] P.A. Nelson, J.M. Elliott, G.S. Attard, J.R. Owen, Chem. Mater. 14 (2002) 524–529.
[4] M.R. Thuler, R.L. Benbow, Z. Hurych, Phys. Rev. B 27 (1983) 2082.
[5] L. Del Bianco, F. Boscherini, M. Tamisari, F. Spizzo, M. Vittori Antisari, E. Piscopiello, J. Phys. D 41 (2003) 134008.
[6] A.M. Huntz, M. Andrieux, R. Molins, Mater. Sci. Eng. A 415 (2006) 21–32.
[7] K. Sakiyama, K. Koga, T. Seto, M. Hirasawa, T. Orii, J. Phys. Chem. B 108 (2004) 523–529.
[8] A.C. Johnston-Peck, J. Wang, J.B. Tracy, ACS Nano. 3 (2009) 1074–1084.
[9] R. Karmhag, T. Tesfamichael, G.A. Niklasson, E. Wackelgard, M. Nygren, J. Phys. D 34 (2001) 400–406.
[10] V. Singh, V. Srinivas, J. Appl. Phys. 106 (2009) 053910;
V. Singh, V. Srinivas, S. Ram, Philos. Mag. 90 (2010) 1401–1414.
[11] V. Skumryev, S. Stoyanov, Y. Zhang, G. Hadjipanayis, D. Givord, J. Nogues, Nature (London) 423 (2003) 850–853.
[12] F. Davara, Z. Fereshteha, M. Salavati-NiasariK, J. Alloys Compd. 476 (2009) 797–801.
[13] S. Li, M. Liu, H. Bi, L. Lu, W. Zou, Z. Huang, Y. Du, J. Alloys Compd. 425 (2006) 1–3.
[14] A.C. Dodd, Powder Technol. 196 (2009) 30–35.
[15] C. Parada, E. Moran, Chem. Mater. 18 (2006) 2719.
[16] A. Roy, V. Srinivas, S. Ram, J.A. De Toro, U. Mizutani, Phys. Rev. B 71 (2005) 184443.
[17] A. Ceylan, C.C. Baker, S.K. Hasanain, S. Ismat Shah, J. Appl. Phys. 100 (2006) 034301.
[18] P. Song, D. Wen, Z.X. Guob, T. Korakianitis, Phys. Chem. Chem. Phys. 10 (2008) 5057–5065.
[19] R. Karmhag, G.A. Niklasson, M. Nygren, J. Appl. Phys. 89 (2001) 3012.
[20] C. Suryanarayana, Prog. Mater. Sci. 46 (2000) 1–184.
[21] H.M. Rietveld, J. Appl. Crystallogr. 2 (1969) 65–71.
[22] G.K. Williamson, W.H. Hall, Acta Metallogr. 1 (1953) 22.
[23] L. Lutterotti, P. Scardi, P. Maistrelli, J. Appl. Crystallogr. 25 (1992) 459.
[24] B.C. Sales, M.B. Maple, Phys. Rev. Lett. 39 (1977) 1636.
[25] B.C. Sales, M.B. Maple, F.L. Vernon, Phys. Rev. B 18 (1978) 486.
[26] J.R. Childress, C.L. Chien, A.F. Jankowski, Phys. Rev. B 45 (1992) 2855.
[27] J.M. Leger, C. Loriers-Susse, B. Vodar, Phys. Rev. B 6 (1972) 4250.
[28] M.B. Stearns, Y. Cheng, J. Appl. Phys. 75 (1994) 6894.